Hindawi
Journal of Control Science and Engineering
Volume 2018, Article ID 3193405, 15 pages
https://doi.org/10.1155/2018/3193405

Research Article

Research on Integrated Guidance and Control of Distributed Cooperation of Multi-Interceptor with State Coupling

Xiang Liu and Xiaogeng Liang

School of Automation, Northwestern Polytechnical University, Xi'an 710072, China

Correspondence should be addressed to Xiang Liu; lx861002@163.com

Received 17 March 2018; Revised 8 June 2018; Accepted 3 July 2018; Published 1 August 2018

Academic Editor: Ai-Guo Wu

With the aim of achieving cooperative target interception by using multi-interceptor, a distributed cooperative control algorithm of the multi-interceptor with state coupling is proposed based on the IGC (integrated guidance and control) method. Considering the coupling relationship between the pitch and ya w channels, a state coupling "leader" IGC model is established, an FTDO (finite-time disturbance observer) is designed for estimating the unknown interference of the model, and the "leader" controller is designed according to the adaptive dynamic surface sliding-mode control law. Secondly, the cooperative control strategy of the multi-interceptor is designed with the "leader-follower" distributed network mode to obtain the speed in the three directions of the interceptor in air and transform them to the general flight speed, trajectory inclination angle, and trajectory deflection instruction by using the transformational relation of kinematics. Finally, the "follower" controller is designed with the FTDO and dynamic surface sliding-mode control. The designed multi-interceptor distributed cooperative IGC algorithm with state coupling has good stability according to the simulation results of two different communication topologies.

1. Introduction

With the rapid development of antimissile technology, it is getting difficult for a single interceptor to break through the defense and intercept targets efficiently, thus making it hard for an interceptor to adapt to the demands of future battlefield scenarios. Therefore, an interceptor with cooperative target interception capability would be more suitable for the future. Multi-interceptor can realize functional complementation through information interaction and sharing, which can not only considerably enhance defense penetration and counterforce of the interceptor but also finish tasks that cannot be achieved by a single interceptor [1].

With respect to cooperative guidance and control of multi-interceptors, the authors in [2, 3] proposed a guidance law with controllable attack time and angle-of-attack constraint and applied it to the salvo attack of anti-ship missiles. Based on this idea, researchers subsequently introduced some other guidance and control methods, including sliding-mode control [4, 5], optimal control [6], differential game [7], and dynamic surface control [8]. This group of methods relies on specifying the attack time before launching to achieve coordination. No information exchange occurs between missiles during flight; hence, these methods apparently have temporal limitations. With the progress in consensus of multiagent systems, researchers have begun to use the consensus theory to study the cooperative guidance and control of multi-interceptors. Using the coordination strategy under the cooperative guidance framework, the authors in [9] adjusted missile trajectories, such that the coordination variable of each missile can approach the expected coordination variable and realize cooperative guidance. The authors in [10] applied the "leader-follower" formation control to cooperative guidance of multi-interceptors by putting forward an analogous "leader-follower" cooperative guidance framework. The authors in [11, 12] explored the guidance and control law of the "leader-follower" topology with angle constraint and topology switch present. By constructing an integrated cost function for multiple missiles, the authors in [13] designed a cooperative guidance law for multiple missiles intercepting a maneuvering target. However, the application of this integrated cost function was faced with multiple constrains because each missile required the global information of all the participating partners.

The interceptor guidance and control system is a highly dynamic, strong-coupling, varying, and uncertain multivariant system featuring complicated dynamic characteristics. Therefore, the integrated guidance and control (IGC) design method can allocate the control ability of interceptors more properly. It mainly generates control power according to the relative motive between the interception targets and the interceptors and then drives the interceptors to chase the targets. Moreover, it cannot only stabilize flight attitude but also enhance guidance precision [14]. In recent years, many researchers worldwide conducted studies focusing on the design method of IGC. The authors in [15, 16] designed an IGC control law with the sliding control mode and back-stepping control algorithm. The sliding-mode control method has been widely used in the design of IGC of aircraft [17], missile [18], and unmanned helicopter [19, 20]. In existing papers, most of them were designed in a single channel [21, 22], regardless of the coupling between channels. The authors in [23, 24] designed IGC algorithms in three dimensions, but designing the controller is difficult when establishing the model with a high order.

According to the above literature review, the guidance loop and control loop of the multi-interceptor cooperative guidance and control have been studied separately by experts. However, external disturbance and its coupling relation during the multi-interceptor flight cannot be ignored. In the meantime, multi-interceptor needs to communicate during its flight to finish cooperative control. Thus, unsmooth local communication should be considered while designing the controller. In light of this, a distributed cooperative control strategy was introduced on top of the integrated guidance and control (IGC) method by considering the coupling between the interception pitch and yaw channels, a design method of cooperative IGC of the multi-interceptor with state coupling of the "leader-follower" distributed topology structure is proposed. The design of the "leader" and "follower" control algorithm using the dynamic surface sliding-mode and finite-time disturbance observer can effectively enhance the stability of the interceptor during the flight and furthermore ensure the target to be hit by the "leader" and "follower" simultaneously following the distributed cooperative controlling strategy. The proposed method can enhance the stability of cooperative guidance and control of the multi-interceptor.

2. "Leader" IGC Model of Interceptor with State Coupling

According to the relative motion relation between the interceptor "leader" and target [25, 26], the relative motion model of the interceptor "leader" and target is established as follows:

$$\begin{aligned} r\ddot{q}_\varepsilon &= -2\dot{r}\dot{q}_\varepsilon - r\dot{q}_\beta^2 \sin q_\varepsilon \cos q_\varepsilon - a_{t\varepsilon} - a_{m4\varepsilon} \\ \ddot{r} &= r\dot{q}_\varepsilon^2 + r\dot{q}_\beta^2 \cos^2 q_\varepsilon + a_{tr} - a_{m4r} \\ -r\ddot{q}_\beta \cos q_\varepsilon &= 2\dot{r}\dot{q}_\beta \cos q_\varepsilon - 2r\dot{q}_\varepsilon \dot{q}_\beta \sin q_\varepsilon + a_{t\beta} - a_{m4\beta} \end{aligned} \tag{1}$$

In the equation, q_β and q_ε denote the elevation angle and horizontal sight angle of the "leader" and target, respectively; $a_{m4\varepsilon}$ and $a_{m4\beta}$ denote the longitudinal and lateral motion acceleration of the "leader," respectively; $a_{t\varepsilon}$ and $a_{t\beta}$ denote the longitudinal and lateral motion acceleration of the target, respectively; r represents the relative distance between the "leader" and target.

The kinetic model of the interceptor "leader" can be indicated as follows:

$$\begin{aligned} \dot{\alpha} &= \omega_z + \omega_y \tan\beta \sin\alpha - \frac{qSC_y^\alpha \alpha \cos\alpha}{mV_m \cos\beta} + d_\alpha \\ \dot{\beta} &= \omega_y \cos\alpha + \frac{qSC_y^\alpha \alpha \sin\alpha \sin\beta}{mV_m} + \frac{qSC_z^\beta \beta \cos\beta}{mV_m} \\ &\quad + d_\beta \\ \dot{\omega}_z &= \frac{q\bar{S}\bar{L}m_z^\alpha \alpha}{J_z} + \frac{q\bar{S}\bar{L}m_z^{\omega_z}\omega_z}{J_z} + \frac{M_z}{J_z} + d_{\omega_z} \\ \dot{\omega}_y &= \frac{q\bar{S}\bar{L}m_y^\beta \beta}{J_y} + \frac{q\bar{S}\bar{L}m_y^{\omega_y}\omega_y}{J_y} + \frac{M_y}{J_y} + d_{\omega_y} \end{aligned} \tag{2}$$

$$\begin{aligned} a_{m3\varepsilon} &= \frac{qSC_y^\alpha \alpha}{m} \\ a_{m3\beta} &= \frac{qSC_z^\beta \beta}{m} \end{aligned} \tag{3}$$

In the equation, S is the reference area of the "leader;" $\bar{L}$ is the reference length of the "leader;" m is the mass of the "leader;" α and β are the attack angle and sideslip angle, respectively; ω_z and ω_y are the pitch angular velocity and yaw rate, respectively; and d_α, d_{ω_z}, d_β, and d_{ω_y} are the disturbance and uncertain disturbance of the various links of the system. J_z and J_y are the rotational inertia; C_y^α, C_z^β, m_z^α, $m_z^{\omega_z}$, m_y^β, and $m_y^{\omega_y}$ are the related aerodynamic force and torque coefficient, respectively; M_z and M_y are the pitch moment and yawing moment of the "leader," respectively; and $a_{m3\varepsilon}$ and $a_{m3\beta}$ are the longitudinal and lateral acceleration of the "leader."

Assuming that the sight angle of the interceptor in the terminal guidance stage changes slightly and the included angle of the sight angle and velocity direction of the interceptor are relatively small, let $a_{m3\varepsilon} = a_{m4\varepsilon}$ and $a_{m3\beta} = a_{m4\beta}$. By defining $x_1 = [\dot{q}_\varepsilon, \dot{q}_\beta]^T$, $x_2 = [\alpha, \beta]^T$, and $x_3 = [\omega_z, \omega_y]^T$, the nonlinear model of the "leader" IGC of the interceptor with state coupling can be obtained, according to (1), (2), and (3).

$$\begin{aligned} \dot{x}_1 &= f_1(x_1) + g_{11}(x_1)x_2 + g_{12}(x_1)a_t \\ \dot{x}_2 &= f_2(x_2) + g_2(x_2)x_3 + d_2 \\ \dot{x}_3 &= f_3(x_2, x_3) + g_3 u + d_3 \\ y &= x_1 \end{aligned} \tag{4}$$

In the equation,

$$f_1(x_1) = \left[-\frac{2\dot{r}}{r}\dot{q}_\varepsilon - \dot{q}_\beta^2 \sin q_\varepsilon \cos q_\varepsilon, -\frac{2\dot{r}}{r}\dot{q}_\beta + 2\dot{q}_\varepsilon \dot{q}_\beta \tan q_\varepsilon\right]^T,$$

$$f_2(x_2) = \left[-\frac{qSC_y^\alpha \alpha \cos\alpha}{mV_m \cos\beta}, \frac{qSC_y^\alpha \alpha \sin\alpha \sin\beta}{mV_m} + \frac{qSC_z^\beta \beta \cos\beta}{mV_m}\right]^T,$$

$$f_3(x_2, x_3) = \left[\frac{qS\bar{L}m_z^\alpha \alpha}{J_z} + \frac{qS\bar{L}m_z^{\omega_z}\omega_z}{J_z}, \frac{qS\bar{L}m_y^\beta \beta}{J_y} + \frac{qS\bar{L}m_y^{\omega_y}\omega_y}{J_y}\right]^T$$

$$g_{11}(x_1) = \begin{bmatrix} -\frac{qSC_y^\alpha}{mr} & 0 \\ 0 & \frac{qSC_z^\beta}{mr\cos q_\varepsilon} \end{bmatrix}, \quad (5)$$

$$g_{12}(x_1) = \begin{bmatrix} \frac{1}{r} & 0 \\ 0 & \frac{1}{r\cos q_\varepsilon} \end{bmatrix},$$

$$g_2(x_2) = \begin{bmatrix} 1 & \tan\beta \sin\alpha \\ 0 & \cos\alpha \end{bmatrix},$$

$$g_3 = \mathrm{diag}\left\{J_z^{-1}, J_y^{-1}\right\},$$

$$u = \left[M_z, M_y\right]^T,$$

$$a_t = \left[a_{t\varepsilon}, -a_{t\beta}\right]^T,$$

$$d_2 = \left[d_\alpha, d_\beta\right]^T,$$

$$d_3 = \left[d_{\omega_z}, d_{\omega_y}\right]^T$$

The unknown disturbances d_2 and d_3 in the "leader" IGC model are assumed to be continuously differentiable and the first-order derivative is bounded. $d_i < N$, $i = 2, 3, N$ is a positive constant.

3. Design of Interceptor "Leader" Controller

3.1. Design of Finite-Time Disturbance Observer. Aiming at the uncertainty a_t, d_2, and d_3 included in the system model (4), an FTDO (finite-time disturbance observer) is designed for estimating unknown disturbances, in order to eliminate the impact of unknown disturbances on the leader system of the interceptor. Define $v_r = \dot{r}$, $v_\varepsilon = r\dot{q}_\varepsilon$, $v_\beta = r\dot{q}_\beta \cos q_\varepsilon$, and

$$\begin{aligned}\dot{v}_\varepsilon &= \dot{r}\dot{q}_\varepsilon + r\ddot{q}_\varepsilon = -\dot{r}\dot{q}_\varepsilon - r\dot{q}_\beta^2 \sin q_\varepsilon \cos q_\varepsilon + a_{t\varepsilon} - a_{m4\varepsilon} \\ &= -\frac{v_r v_\varepsilon}{r} - \frac{v_\beta^2 \tan q_\varepsilon}{r} + a_{t\varepsilon} - a_{m4\varepsilon}\end{aligned} \quad (6)$$

$$\begin{aligned}\dot{v}_\beta &= \dot{r}\dot{q}_\beta \cos q_\varepsilon + r\ddot{q}_\beta \cos q_\varepsilon - r\dot{q}_\varepsilon \dot{q}_\beta \sin q_\varepsilon \\ &= -\dot{r}\dot{q}_\beta \cos q_\varepsilon + r\dot{q}_\varepsilon \dot{q}_\beta \sin q_\varepsilon - a_{t\beta} + a_{m4\beta} \\ &= -\frac{v_r v_\beta}{r} + \frac{v_\varepsilon v_\beta \tan q_\varepsilon}{r} - a_{t\beta} + a_{m4\beta}\end{aligned} \quad (7)$$

Define $w_1 = [v_\varepsilon, v_\beta]^T$, and according to (6) and (7),

$$\dot{w}_1 = h_1(w_1) + h_2(w_1)\, x_2 + a_t \quad (8)$$

In the equation,

$$h_1(w_1) = \begin{bmatrix} -\frac{v_r v_\varepsilon}{r} - \frac{v_\beta^2 \tan q_\varepsilon}{r} \\ -\frac{v_r v_\beta}{r} + \frac{v_\varepsilon v_\beta \tan q_\varepsilon}{r} \end{bmatrix},$$

$$h_2(w_1) = \begin{bmatrix} -\frac{qSC_y^\alpha \alpha}{m} & 0 \\ 0 & \frac{qSC_z^\beta \beta}{m} \end{bmatrix} \quad (9)$$

The following FTDO is designed to estimate the acceleration a_t of the target, and

$$\begin{aligned}\dot{z}_{10} &= v_{10} + h_1(w_1) + h_2(w_1)\, x_2, \\ \dot{z}_{11} &= v_{11}, \\ \dot{z}_{12} &= v_{12} \\ v_{10} &= -\lambda_{10}\left[L_1^{1/3}\left|z_{10} - w_1\right|^{2/3} \mathrm{sgn}\left(z_{10} - w_1\right)\right] + z_{11} \\ v_{11} &= -\lambda_{11}\left[L_1^{1/2}\left|z_{11} - v_{10}\right|^{1/2} \mathrm{sgn}\left(z_{11} - v_{10}\right)\right] + z_{12} \\ v_{12} &= -\lambda_{12}\left[L_1\left|z_{12} - v_{11}\right|^{q_1/p_1} \mathrm{sgn}\left(z_{12} - v_{11}\right)\right] \\ z_{10} &= \widehat{w}_1, \\ z_{11} &= \widehat{a}_t, \\ z_{12} &= \dot{\widehat{a}}_t\end{aligned} \quad (10)$$

In the equation $w_1 = [w_{11}, w_{12}]^T$, $z_{10} = [z_{101}, z_{102}]^T$, $z_{11} = [z_{111}, z_{112}]^T$, $z_{12} = [z_{121}, z_{122}]^T$, $v_{10} = [v_{101}, v_{102}]^T$, $v_{11} = [v_{111}, v_{112}]^T$, $v_{12} = [v_{121}, v_{122}]^T$, $L_1 = [L_{11}, L_{12}]^T$, $\widehat{a}_t$ is the estimated acceleration a_t of the target, the estimated value w_1 and $\dot{a}_t$ is $\widehat{w}_1$ and $\dot{\widehat{a}}_t$, λ_{10}, λ_{11}, and λ_{12} are the coefficients to be designed for the disturbance observer, q_1 and p_1 are the terminal coefficients, respectively, and $0 < p_1 < q_1$.

It can be learnt according to [27] that appropriate parameters can guarantee that the FTDO error system is steady in finite time. The estimated error of the acceleration a_t of the target is defined as $e_{11} = z_{11} - a_t$.

Similarly, the disturbance d_2 and d_3 of the second subsystem and third subsystem is estimated, and

$$\begin{aligned}
\dot{z}_{20} &= v_{20} + f_2(x_2) + g_2(x_2)x_3,\\
\dot{z}_{21} &= v_{21},\\
\dot{z}_{22} &= v_{22}\\
v_{20} &= -\lambda_{20}\left[L_2^{1/3}\left|z_{20} - x_2\right|^{2/3}\operatorname{sgn}(z_{20} - x_2)\right] + z_{21}\\
v_{21} &= -\lambda_{21}\left[L_2^{1/2}\left|z_{21} - v_{20}\right|^{1/2}\operatorname{sgn}(z_{21} - v_{20})\right] + z_{22}\\
v_{22} &= -\lambda_{22}\left[L_2\left|z_{22} - v_{21}\right|^{q_2/p_2}\operatorname{sgn}(z_{22} - v_{21})\right]\\
z_{20} &= \hat{x}_2,\\
z_{21} &= \hat{d}_2,\\
z_{22} &= \dot{\hat{d}}_2
\end{aligned} \tag{11}$$

$$\begin{aligned}
\dot{z}_{30} &= v_{30} + f_3(x_2, x_3) + g_3 u,\\
\dot{z}_{31} &= v_{31},\\
\dot{z}_{32} &= v_{32}\\
v_{30} &= -\lambda_{30}\left[L_3^{1/3}\left|z_{30} - x_3\right|^{2/3}\operatorname{sgn}(z_{30} - x_3)\right] + z_{31}\\
v_{31} &= -\lambda_{31}\left[L_3^{1/2}\left|z_{31} - v_{30}\right|^{1/2}\operatorname{sgn}(z_{31} - v_{30})\right] + z_{32}\\
v_{32} &= -\lambda_{32}\left[L_3\left|z_{32} - v_{31}\right|^{q_3/p_3}\operatorname{sgn}(z_{32} - v_{31})\right]\\
z_{30} &= \hat{x}_3,\\
z_{31} &= \hat{d}_3,\\
z_{32} &= \dot{\hat{d}}_3
\end{aligned} \tag{12}$$

In the equation, the estimated value of disturbance d_2 and d_3 is $\hat{d}_2$ and $\hat{d}_3$, respectively, and the estimated error is $e_{21} = z_{21} - d_2$ and $e_{31} = z_{31} - d_3$, respectively.

3.2. Design of Adaptive Dynamic Sliding-Mode Controller. Because the interceptor IGC model is an unmatched and uncertain system, and aiming at the state coupling IGC model (4) and FTDO estimated value (10)–(12), the "leader" control algorithm is designed by taking advantage of the adaptive dynamic sliding-mode control law.

(1) The command signal of the first subsystem of (4) is defined as x_{1d}. In order to realize the guidance goal, the sight angular velocity should be removed. According to the design method of dynamic surface sliding-mode control, the first dynamic error surface is defined as follows:

$$s_1 = -g_{11}^{-1}(x_1)(x_1 - x_{1d}) \tag{13}$$

Taking the derivative of s_1, the dynamic equation of error is given by

$$\begin{aligned}
\dot{s}_1 = {} & g_{11}^{-2}(x_1)\dot{g}_{11}(x_1)(x_1 - x_{1d})\\
& - g_{11}^{-1}(x_1)\left[f_1(x_1) + g_{12}(x_1)a_t - \dot{x}_{1d}\right] - x_2
\end{aligned} \tag{14}$$

According to the dynamic surface design method and FTDO estimated value $\hat{a}_t$ in (10), the virtual control amount of the first dynamic surface can be obtained as follows:

$$\begin{aligned}
x_2^* = {} & g_{11}^{-2}(x_1)\dot{g}_{11}(x_1)(x_1 - x_{1d})\\
& - g_{11}^{-1}(x_1)\left[f_1(x_1) + g_{12}(x_1)\hat{a}_t - \dot{x}_{1d}\right] + k_1 s_1
\end{aligned} \tag{15}$$

In the equation, $k_1 = \operatorname{diag}\{k_{11}, k_{12}\}$ is the positive definite matrix. In the design process, differential blast would occur, while the differential of the virtual control amount x_2^* is taken. In order to avoid the complicated computation process owing to item inflation, x_2^* must be obtained through the first-order low-pass filter, and the virtual control amount of the filter can be obtained as follows:

$$\begin{aligned}
\tau_2\dot{\bar{x}}_2^* + \bar{x}_2^* &= x_2^*,\\
\bar{x}_2^*(0) &= x_2^*(0)
\end{aligned} \tag{16}$$

In the equation, $\tau_2 = \operatorname{diag}\{\tau_{21}, \tau_{22}\}$ is the time constant of the filter, and the differential of the virtual control after the error surface filter can be obtained.

$$\dot{\bar{x}}_2^* = -\tau_2^{-1}(\bar{x}_2^* - x_2^*) \tag{17}$$

(2) The second dynamic error surface is defined as

$$s_2 = x_2 - \bar{x}_2^* \tag{18}$$

Taking the derivative of s_2, the dynamic equation of error can be obtained as follows:

$$\dot{s}_2 = \dot{x}_2 - \dot{\bar{x}}_2^* = f_2(x_2) + g_2(x_2)x_3 + d_2 - \dot{\bar{x}}_2^* \tag{19}$$

Similar to the first dynamic surface design method, the estimated FTDO value $\hat{d}_2$ is substituted in (11). Thus, the virtual control of the second dynamic surface can be obtained as follows:

$$x_3^* = g_2^{-1}(x_2)\left[-f_2(x_2) - \hat{d}_2 + \dot{\bar{x}}_2^* - k_2 s_2\right] \tag{20}$$

In the equation, $k_2 = \operatorname{diag}\{k_{21}, k_{22}\}$ is the positive definite matrix. Similarly, by obtaining x_3^* through the first-order low-pass filter, the virtual control amount of the filter can be obtained as follows:

$$\begin{aligned}
\tau_3\dot{\bar{x}}_3^* + \bar{x}_3^* &= x_3^*,\\
\bar{x}_3^*(0) &= x_3^*(0)
\end{aligned} \tag{21}$$

In the equation, $\tau_3 = \operatorname{diag}\{\tau_{31}, \tau_{32}\}$ is the time constant of the filter. The differential of virtual control after the error surface filter can be obtained as follows:

$$\dot{\bar{x}}_3^* = -\tau_3^{-1}(\bar{x}_3^* - x_3^*) \tag{22}$$

(3) The third dynamic error surface is defined as follows:

$$s_3 = x_3 - \overline{x}_3^* \tag{23}$$

Taking the derivative of s_3, the dynamic equation of error can be obtained as follows:

$$\dot{s}_3 = \dot{x}_3 - \dot{\overline{x}}_3^* = f_3(x_2, x_3) + g_3 u + d_3 - \dot{\overline{x}}_3^* \tag{24}$$

To guarantee the convergence velocity of the interceptor "leader," an adaptive sliding-mode reaching law is designed:

$$\dot{s} = -k_a \left|\frac{\dot{r}}{r}\right| s - k_b |s|^{\partial} \operatorname{sgn}(s) \tag{25}$$

In the equation, $k_a > 0$, $k_b > 0$, and $\dot{r}$ denotes the change in relative distance between the "leader" and target.

According to (24) and (25) and estimated FTDO $\widehat{d}_3$ of (12), the adaptive dynamic surface sliding-mode control law of the interceptor "leader" is given by

$$\begin{aligned} u = g_3^{-1} \Big[& -f_3(x_2, x_3) - \widehat{d}_3 + \dot{\overline{x}}_3^* - k_3 \left|\frac{\dot{r}}{r}\right| s_3 \\ & - k_4 |s_3|^{\partial} \operatorname{sgn}(s_3) \Big] \end{aligned} \tag{26}$$

In the equation, $k_3 = \operatorname{diag}\{k_{31}, k_{32}\}$, $k_4 = \operatorname{diag}\{k_{41}, k_{42}\}$, and $\partial = \operatorname{diag}\{\partial_{11}, \partial_{12}\}$ are positive definite matrices, and $0 < \partial < 1$.

3.3. Stability Analysis

Theorem 1. *Consider the integrated guidance and control system for the "leader" (equation (4)). If the convergence rate is calculated using (25), the disturbance values of the system (see (4)) are estimated using (10)-(12), and filter equations (16) and (21) are implemented; then finally under the dynamic surface sliding-mode control law (see (26)), imposing the constraint for ensuring the system (see (4)) output error converging into the adjacent area of the origin, an arbitrary adjacent area of the origin can be obtained with the appropriate design parameter determined.*

To prove:

Let us assume that the estimated error of FTDO system meets

$$\begin{aligned} |e_{11}| &< N_1, \\ |e_{21}| &< N_2, \\ |e_{31}| &< N_3 \end{aligned} \tag{27}$$

In the equation, N_1, N_2, and N_3 are positive constants.

The filter error is defined as follows:

$$\begin{aligned} y_2 &= \overline{x}_2^* - x_2^*, \\ y_3 &= \overline{x}_3^* - x_3^* \end{aligned} \tag{28}$$

Taking the derivative of y_2 and y_3, the dynamic error of the filter can be obtained as follows:

$$\begin{aligned} \dot{y}_2 &= -\tau_2^{-1} y_2 - \dot{x}_2^*, \\ \dot{y}_3 &= -\tau_3^{-1} y_3 - \dot{x}_3^* \end{aligned} \tag{29}$$

According to (13)–(23) and (28),

$$\begin{aligned} x_1 &= -g_{11}(x_1) s_1 + x_{1d} \\ x_2 &= s_2 + \overline{x}_2^* = s_2 + y_2 + x_2^* \\ x_3 &= s_4 + \overline{x}_3^* = s_3 + y_3 + x_3^* \end{aligned} \tag{30}$$

According to (4), (11)–(21), and (26)–(28),

$$\begin{aligned} \dot{s}_1 &= g_{11}^{-2}(x_1) \dot{g}_{11}(x_1)(x_1 - x_{1d}) \\ &\quad - g_{11}^{-1}(x_1) [f_1(x_1) + g_{12}(x_1) a_t - \dot{x}_{1d}] - x_2 \\ &= -s_2 - y_2 - k_1 s_1 + \widetilde{e}_{11} \end{aligned} \tag{31}$$

In the equation, $\widetilde{e}_{11} = g_{11}^{-1}(x_1) g_{12}(x_1) e_{11}$. Let us assume that $|\widetilde{e}_{11}| < \widetilde{N}_1$, where $\widetilde{N}_1$ is a positive constant.

$$\begin{aligned} \dot{s}_2 &= \dot{x}_2 - \dot{\overline{x}}_2^* = f_2(x_2) + g_2(x_2) x_3 + d_2 - \dot{\overline{x}}_2^* \\ &= g_2(x_2)(s_3 + y_3) - k_2 s_2 - e_{21} \end{aligned} \tag{32}$$

$$\begin{aligned} \dot{s}_3 &= \dot{x}_3 - \dot{\overline{x}}_3^* = f_3(x_2, x_3) + g_3 u + d_3 - \dot{\overline{x}}_3^* \\ &= -k_3 \left|\frac{\dot{r}}{r}\right| s_3 - k_4 |s_3|^{\partial} \operatorname{sgn}(s_3) - e_{31} \end{aligned} \tag{33}$$

According to Young's equation and (30)–(33),

$$\begin{aligned} s_1^T \dot{s}_1 &= s_1^T (-s_2 - y_2 - k_1 s_1 + \widetilde{e}_{11}) \\ &\le s_1^T \left(\frac{3}{2} I - k_1\right) s_1 + \frac{1}{2} s_2^T s_2 + \frac{1}{2} y_2^T y_2 + \frac{1}{2} \widetilde{N}_1^2 \end{aligned} \tag{34}$$

$$\begin{aligned} s_2^T \dot{s}_2 &= s_2^T [g_2(x_2)(s_3 + y_3) - k_2 s_2 - e_{21}] \\ &\le s_2^T \left(\frac{1}{2} I + g_2^2 - k_2\right) s_2 + \frac{1}{2} s_3^T s_3 + \frac{1}{2} y_3^T y_3 \\ &\quad + \frac{1}{2} N_2^2 \end{aligned} \tag{35}$$

$$\begin{aligned} s_3^T \dot{s}_3 &= s_3^T \left(-k_3 \left|\frac{\dot{r}}{r}\right| s_3 - k_4 |s_3|^{\partial} \operatorname{sgn}(s_3) - e_{31}\right) \\ &\le s_3^T \left(\frac{1}{2} I - k_3 + \frac{3}{2} k_4\right) s_3 + \frac{1}{2} N_3^2 + \frac{1}{2} k_4 \end{aligned} \tag{36}$$

It can be learnt that variables and their differential in the system model are bounded, and there are continuous functions $\widetilde{z}_2$ and $\widetilde{z}_3$, where $\widetilde{z}_2 > 0$ and $\widetilde{z}_3 > 0$, enabling variables $\dot{x}_2^*$ and $\dot{x}_3^*$ to meet

$$\begin{aligned} |\dot{x}_2^*| &\le \widetilde{z}_2, \\ |\dot{x}_3^*| &\le \widetilde{z}_3 \end{aligned} \tag{37}$$

According to Young's equation and (28)–(29) and (37):

$$y_2^T \dot{y}_2 = y_2^T \left(-\tau_2^{-1} y_2 - \dot{x}_2^*\right) \leq y_2^T \left(\frac{1}{2} I - \tau_2^{-1}\right) y_2 + \frac{1}{2}\widetilde{z}_2^2 \quad (38)$$

$$y_3^T \dot{y}_3 = y_3^T \left(-\tau_3^{-1} y_3 - \dot{x}_3^*\right) \leq y_3^T \left(\frac{1}{2} I - \tau_3^{-1}\right) y_3 + \frac{1}{2}\widetilde{z}_3^2 \quad (39)$$

According to the state coupling IGC nonlinear system model (4), a Lyapunov function is selected:

$$V = \frac{1}{2}\left(s_1^T s_1 + s_2^T s_2 + s_3^T s_3 + y_2^T y_2 + y_3^T y_3\right) \quad (40)$$

Taking the derivative of (40),

$$\begin{aligned}
\dot{V} &= s_1^T \dot{s}_1 + s_2^T \dot{s}_2 + s_3^T \dot{s}_3 + y_2^T \dot{y}_2 + y_3^T \dot{y}_3 \\
&\leq s_1^T \left(\frac{3}{2} I - k_1\right) s_1 + \frac{1}{2} s_2^T s_2 + \frac{1}{2} y_2^T y_2 + \frac{1}{2}\widetilde{N}_1^2 \\
&\quad + s_2^T \left(\frac{1}{2} I + g_2^2 - k_2\right) s_2 + \frac{1}{2} s_3^T s_3 + \frac{1}{2} y_3^T y_3 \\
&\quad + \frac{1}{2} N_2^2 + s_3^T \left(\frac{1}{2} I - k_3 + \frac{3}{2} k_4\right) s_3 + \frac{1}{2} N_3^2 + \frac{1}{2} k_4 \\
&\quad + y_2^T \left(\frac{1}{2} I - \tau_2^{-1}\right) y_2 + \frac{1}{2}\widetilde{z}_2^2 + y_3^T \left(\frac{1}{2} I - \tau_3^{-1}\right) y_3 \\
&\quad + \frac{1}{2}\widetilde{z}_3^2
\end{aligned} \quad (41)$$

The design parameters meet the following rules:

$$\begin{aligned}
k_1 &\geq \frac{3}{2} I + \frac{1}{2}\kappa I, \\
k_2 &\geq I + g_2^2 + \frac{1}{2}\kappa I, \\
k_3 &\geq I + \frac{3}{2} k_4 + \frac{1}{2}\kappa I \\
\tau_2^{-1} &\geq I + \frac{1}{2}\kappa I, \\
\tau_3^{-1} &\geq I + \frac{1}{2}\kappa I
\end{aligned} \quad (42)$$

In the equation, κ is a constant, and $\kappa > 0$. Therefore,

$$\dot{V} \leq -\kappa V + \widehat{A} \quad (43)$$

In the equation, $\widehat{A} = (1/2)\widetilde{N}_1^2 + (1/2)N_2^2 + (1/2)N_3^2 + (1/2)\widetilde{z}_2^2 + (1/2)\widetilde{z}_3^2 + (1/2)k_4$.

According to (43),

$$V(t) \leq \frac{\left\{\left[\kappa V(0) - \widehat{A}\right] e^{-\kappa t} + \widehat{A}\right\}}{\kappa} \quad (44)$$

s_1, s_2, s_3, y_2, and y_3 are consistent and eventually bounded. Thus, large parameters k_1, k_2, k_3, and k_4, as well as small parameters τ_2 and τ_3 are selected, to make the value of κ sufficiently large and $\widehat{A}/\kappa$ sufficiently small to ensure control precision.

Remark 2. Theoretically, the final boundaries of error surfaces s_1, s_2, and s_3 and filter errors y_2 and y_3 will become smaller with the increasing design parameters k_1, k_2, k_3, and k_4 and the decreasing τ_2 and τ_3. This change leads to a higher controlling precision. However, in reality, using too large parameters (k_1, k_2, k_3, and k_4) and too small parameters (τ_2 and τ_3) will result in an input saturation for the interceptor control system. The nonlinear behavior of the saturated system results in a higher requirement of overload exceeding the available overload. Therefore, the angle of attack and the sideslip angle of the interceptor exceed the allowable range leading to a reduced controlling performance of the system. Furthermore, the physical constraints of the low-pass filter prohibit parameters τ_2 and τ_3 from being too small. Therefore, the parameters of the control algorithm should be properly selected by combining practical situations.

4. Distributed Network Synchronization Strategy

4.1. Design of Cooperative Control Strategy Based on the Distributed Network. Based on the principle of time consistency of a multiagent system, the multi-interceptor cooperative control strategy is designed to ensure that all interceptors hit the targets at the same time. In the cooperative system of the multi-interceptor, the state information of other interceptors can be obtained through information interaction, for realizing time consistency, and such information interaction can be described using the graph theory. Assuming that each interceptor is a communication node, the information exchange among interceptors can be indicated as $\overline{G} = \{\overline{V}, \overline{E}, \overline{A}\}$, where $\overline{V} = \{\overline{v}_i,\ i = 1, 2, \ldots, n\}$ denotes the set of interceptor nodes and $\overline{E}$ denotes the lines between the interceptor nodes. The weighted coefficient matrix is indicated as $\overline{A} = [\overline{a}_{ij}] \in \mathbb{R}^{n\times n}$; $\overline{a}_{ij} > 0$ implies that the interceptor node i and node j can exchange information. However, if $\overline{a}_{ij} = 0$, information cannot be exchanged. $\overline{L}$ denotes the Laplace matrix of the undirected graph $\overline{G}$, among which the elements satisfy

$$\begin{aligned}
\overline{l}_{ii} &= \sum_{j=1, j\neq i}^{n} \overline{a}_{ij} \\
\overline{l}_{ij} &= -\overline{a}_{ij}, \quad j \neq i
\end{aligned} \quad (45)$$

$\overline{B} = \mathrm{diag}\{\overline{b}_1, \overline{b}_2, \ldots, \overline{b}_j\}$ denotes whether the interceptors can obtain the state information of the leader, $\overline{b}_i > 0$, $i \in \{1, 2, 3, \ldots, j\}$ indicates that the interceptors can obtain the state information of the leader, and $\overline{b}_i = 0$, $i \in \{1, 2, 3, \ldots, j\}$ indicates that the interceptors cannot obtain the state information of the leader.

Based on the "leader-follower" topology structure, the distributed cooperative control strategy of the multi-interceptor is designed as follows:

$$v_i = \overline{k}_{i1}\left[\sum_{j=1}^{n} \overline{a}_{ij}\left(\varsigma_j - \varsigma_i\right) + \overline{b}_i\left(\varsigma_0 - \varsigma_i\right)\right] + \dot{\varsigma}_0 \quad (46)$$

In the equation, $\varsigma_0 = [x_0, y_0, z_0]^T$ denotes the position of the "leader," $\varsigma_i = [x_i, y_i, z_i]^T$, $i \in \{1, 2, 3, \ldots, j\}$ denotes the position of the interceptors, $v_i = \dot{\varsigma}_i$, $i \in \{1, 2, 3, \ldots, j\}$ denotes the velocity of the interceptors, $\overline{k}_{i1} = \text{diag}\{\overline{k}_{i11}, \overline{k}_{i12}, \overline{k}_{i13}\}$ is a constant, and $\overline{k}_{i1} > 0$.

Theorem 3. *If the "follower" state of the interceptor can converge to the "leader" state following the cooperative control strategy (see (46)), such cooperative strategy is then considered to be successful.*

To prove:

Lemma 4. *Laplace matrix $\overline{M}$ has the following properties:*

(1) If $\overline{G}$ is connected, the characteristic value of $\overline{M}$ is $\lambda_{min}(\overline{M}) > 0$, and it is called the algebraic connectivity of the network-connected graph. The larger the value of $\lambda_{min}(\overline{M})$, the more connected the network.

(2) One of the characteristic values of $\overline{M}$ is 0, and its corresponding characteristic vector is $\mathbf{1}$.

The error variable is defined as $e_i = \varsigma_i - \varsigma_0$, and

$$\dot{e}_i = \dot{\varsigma}_i - \dot{\varsigma}_0 = k_{i1}\left(\sum_{j=1}^{n} \overline{a}_{ij}\left(e_j - e_i\right) + \overline{b}_i e_i\right) \tag{47}$$

The Lyapunov function is defined as

$$V = \frac{1}{2} e^T \left(\overline{M} + \overline{B}\right) e \tag{48}$$

In the equation, $e = [e_1, e_2, \ldots, e_n]^T$.

$\overline{k}_i = \min\{\overline{k}_{i1}\}$, and taking the derivative of the above equation,

$$\begin{aligned}
\dot{V} &= \dot{e}^T \left(\overline{M} + \overline{B}\right) e = -\sum_{i=1}^{n}\left[\sum_{j=1}^{n} a_{ij}\left(e_j - e_i\right) - \overline{b}_i e_i\right]\dot{e}_i \\
&= -\sum_{i=1}^{n} \overline{k}_{i1}\left[\sum_{j=1}^{n} a_{ij}\left(e_j - e_i\right) - \overline{b}_i e_i\right] \\
&\cdot \left(\sum_{j=1}^{n} \overline{a}_{ij}\left(e_j - e_i\right) + \overline{b}_i e_i\right) = -\sum_{i=1}^{n} \overline{k}_{i1} \\
&\cdot \left[\sum_{j=1}^{n} a_{ij}\left(e_j - e_i\right) - \overline{b}_i e_i\right]^2 \\
&\le -\overline{k}_i \sum_{i=1}^{n}\left[\sum_{j=1}^{n} a_{ij}\left(e_j - e_i\right) - \overline{b}_i e_i\right]^2
\end{aligned} \tag{49}$$

Let $V(e) \neq 0$. Then, according to the above equation,

$$\begin{aligned}
&\frac{\sum_{i=1}^{n}\left[\sum_{j=1}^{n} a_{ij}\left(e_j - e_i\right) - \overline{b}_i e_i\right]^2}{V(e)} \\
&= \frac{e^T\left(\overline{M} + \overline{B}\right)^T\left(\overline{M} + \overline{B}\right)e}{(1/2)\left(e^T\left(\overline{M} + \overline{B}\right)^T e\right)} \ge 2\lambda_{\min}\left(\overline{M} + \overline{B}\right)
\end{aligned} \tag{50}$$

According to (49)–(50),

$$\dot{V}(t) \le -\overline{k}_i\left[2\lambda_{\min}\left(\overline{M} + \overline{B}\right)\right] \tag{51}$$

Therefore, $V(t)$ is convergent in finite time, namely, the convergence state from the "follower" to the "leader"; it can realize cooperative guidance and control of the multi-interceptor.

4.2. Implementation of Distributed Network Cooperative Control Strategy. In order to implement the distributed network synchronization strategy, instructions provided to the synchronization strategy should be traced for each interceptor "follower." The motion relation of the interceptors involved in cooperative interception is given as follows:

$$\begin{aligned}
\dot{x}_i &= V_{mi}\cos\theta_{mi}\cos\varphi_{mvi} \\
\dot{y}_i &= V_{mi}\sin\theta_{mi} \\
\dot{z}_i &= -V_{mi}\cos\theta_{mi}\sin\varphi_{mvi}
\end{aligned} \tag{52}$$

In the equation, $\dot{x}_i$, $\dot{y}_i$, and $\dot{z}_i$ are the velocity components of the ith interceptor in the inertial frame, and θ_{mi} and φ_{mvi} are the trajectory inclination angle and trajectory deflection angle of the ith interceptor.

According to the distributed network synchronization strategy (46), the velocity reference instruction of the interceptor is given by

$$\begin{aligned}
\overline{V}_{mxi} &= \overline{k}_{i1}\left(\sum_{j=1}^{n} \overline{a}_{ij}\left(x_j - x_i\right) + \overline{b}_i\left(x_m - x_i\right)\right) + \dot{x}_m \\
\overline{V}_{myi} &= \overline{k}_{i1}\left(\sum_{j=1}^{n} \overline{a}_{ij}\left(y_j - y_i\right) + \overline{b}_i\left(y_m - y_i\right)\right) + \dot{y}_m \\
\overline{V}_{mzi} &= \overline{k}_{i1}\left(\sum_{j=1}^{n} \overline{a}_{ij}\left(z_j - z_i\right) + \overline{b}_i\left(z_m - z_i\right)\right) + \dot{z}_m
\end{aligned} \tag{53}$$

According to (52), the total velocity, trajectory inclination angle, and trajectory deflection angle of the interceptor can be obtained as follows:

$$\begin{aligned}
\overline{V}_{mi}^{*} &= \sqrt{\left(\overline{V}_{mxi}\right)^2 + \left(\overline{V}_{myi}\right)^2 + \left(\overline{V}_{mzi}\right)^2} \\
\overline{\theta}_{mi}^{*} &= \arcsin\left(\frac{\overline{V}_{myi}}{\overline{V}_{mi}}\right) \\
\overline{\varphi}_{vmi}^{*} &= -\arctan\left(\frac{\overline{V}_{mzi}}{\overline{V}_{mxi}}\right)
\end{aligned} \tag{54}$$

To obtain the differential of the total velocity and trajectory inclination angle of the tractor $\dot{\overline{x}}$, the signal is obtained through the filter. Let $\overline{x}$ and $\overline{x}_1^*$ be the postfiltering instruction and prefiltering instruction, respectively. Then,

$$\ddot{\overline{x}} = -2\zeta_n\omega_n\dot{\overline{x}} - \omega_n^2\overline{x} + \omega_n^2\overline{x}_1^* \tag{55}$$

In the equation, ζ_n and ω_n are the damping and bandwidth of the filter, respectively.

5. Design of Interceptor "Follower" Controller

The instructions provided by the cooperative control strategy can be transformed into velocity, trajectory inclination angle, and trajectory deflection angle instruction. In order to track the command signal of interceptor "follower" in the cooperative network, the "follower" controller adopts the dynamic surface sliding-mode control algorithm. Assuming that the velocity of the interceptor "follower" is controllable, the flight velocity can be indicated as follows:

$$\dot{V}_m = \frac{\cos\alpha_i\cos\beta_i}{m}P_i - g\sin\theta_{mi} \tag{56}$$

In the equation, P_i is the motor power, m is the quality of "follower", α_i and β_i are the attack angle and sideslip angle, respectively, θ_{mi} is the trajectory inclination angle, and g is the gravitational acceleration.

According to (56), the error surface is defined as follows:

$$s_v = V_m - \overline{V}_{mi} \tag{57}$$

In the equation, $\overline{V}_{mi}$ is the reference velocity command of the "follower" after filtering. Taking the derivative of s_v,

$$\dot{s}_v = \frac{\cos\alpha_i\cos\beta_i}{m}P_i - g\sin\theta_{mi} - \dot{\overline{V}}_{mi} \tag{58}$$

In the equation, $\dot{\overline{V}}_{mi}$ is the differential of total velocity after filtering.

To ensure that the velocity of the "follower" can track the system command rapidly, the following sliding-mode reaching law is adopted:

$$\dot{s} = -k_a s - k_b|s|^{\partial}\operatorname{sgn}(s) \tag{59}$$

According to (56)–(59), the thrust of the "follower" can be obtained as follows:

$$P_i = \frac{m}{\cos\alpha_i\cos\beta_i}\left[\dot{\overline{V}}_{mi} + g\sin\theta_{mi} - k_{v1}s_v - k_{v2}|s_v|^{\partial_v}\operatorname{sgn}(s_v)\right] \tag{60}$$

In the equation, $k_{v1} > 0$, $k_{v2} > 0$, $0 < \partial_v < 1$.

By defining $x_{i1} = [\theta_{mi}, \varphi_{vmi}]^T$, $x_{i2} = [\alpha_i, \beta_i]^T$, and $x_{i3} = [\omega_{zi}, \omega_{yi}]^T$, the state coupling kinetic equations of the ith "follower" can be indicated as follows:

$$\begin{aligned}
\dot{x}_{i1} &= g_{i1}x_{i2} + d_{i1}\\
\dot{x}_{i2} &= f_{i2}(x_{i2}) + g_{i2}(x_{i2})x_{i3} + d_{i2}\\
\dot{x}_{i3} &= f_{i3}(x_{i2}, x_{i3}) + g_{i3}u_i + d_{i3}
\end{aligned} \tag{61}$$

In the equation,

$$\begin{aligned}
f_{i2}(x_{i2}) &= \left[-\frac{qSC_y^{\alpha_i}\alpha_i\cos\alpha_i}{mV_{mi}\cos\beta_i}, \frac{qSC_y^{\alpha_i}\alpha_i\sin\alpha_i\sin\beta_i}{mV_{mi}} + \frac{qSC_z^{\beta_i}\beta_i\cos\beta_i}{mV_{mi}}\right]^T,\\
f_{i3}(x_{i2}, x_{i3}) &= \left[\frac{q\overline{SL}m_z^{\alpha_i}\alpha_i}{J_z} + \frac{q\overline{SL}m_z^{\omega_{zi}}\omega_{zi}}{J_z}, \frac{q\overline{SL}m_y^{\beta_i}\beta_i}{J_y} + \frac{q\overline{SL}m_y^{\omega_{yi}}\omega_{yi}}{J_y}\right]^T\\
g_{i1} &= \begin{bmatrix}-\dfrac{qSC_y^{\alpha_i}}{m} & 0\\ 0 & \dfrac{qSC_z^{\beta i}}{m}\end{bmatrix},\\
g_{i2}(x_{i2}) &= \begin{bmatrix}1 & \tan\beta_i\sin\alpha_i\\ 0 & \cos\alpha_i\end{bmatrix},\\
g_{i3} &= \operatorname{diag}\left\{J_z^{-1}, J_y^{-1}\right\},\\
u_i &= \left[M_{zi}, M_{yi}\right]^T,\\
d_{i1} &= \left[d_{\theta i}, d_{\varphi_{vi}}\right]^T,\\
d_{i2} &= \left[d_{\alpha i}, d_{\beta i}\right]^T,\\
d_{i3} &= \left[d_{\omega_{zi}}, d_{\omega_{yi}}\right]^T
\end{aligned} \tag{62}$$

According to (10)–(12), the following form of FTDO is designed for evaluating the disturbance d_{i1}, d_{i2}, and d_{i3} to (61),

$$\begin{aligned}
\dot{z}_{i10} &= v_{i10} + g_{i1}x_{i2},\\
\dot{z}_{i11} &= v_{i11},\\
\dot{z}_{i12} &= v_{i12}\\
v_{i10} &= -\lambda_{i10}\left[L_{i1}^{1/3}|z_{i10} - x_{i1}|^{2/3}\operatorname{sgn}(z_{i10} - x_{i1})\right] + z_{i11}\\
v_{i11} &= -\lambda_{i11}\left[L_{i1}^{1/2}|z_{i11} - v_{i10}|^{1/2}\operatorname{sgn}(z_{i11} - v_{i10})\right] + z_{i12}\\
v_{i12} &= -\lambda_{i12}\left[L_{i1}|z_{i12} - v_{i11}|^{q_{i1}/p_{i1}}\operatorname{sgn}(z_{i12} - v_{i11})\right]\\
z_{i10} &= \widehat{x}_{i1},
\end{aligned}$$

$$z_{i11} = \widehat{d}_{i1},$$
$$z_{i12} = \dot{\widehat{d}}_{i1} \tag{63}$$

In the equation, the estimated value of d_{i1} is $\widehat{d}_{i1}$, and the estimated error is $e_{i11} = z_{i11} - d_{i1}$.

Similarly, the estimated values of d_{i2} and d_{i3} are $\widehat{d}_{i2}$ and $\widehat{d}_{i3}$, respectively, and the estimated errors are $e_{i12} = z_{i12} - d_{i2}$ and $e_{i13} = z_{i13} - d_{i3}$.

To ensure that the "follower" can track the command signal of the cooperative control strategy rapidly and guarantee steady flight attitude, the "follower" controller is designed with the dynamic surface sliding-mode control law, and according to the FTDO estimated value and state coupling kinetic equation (61).

(1) The first dynamic error surface is defined as follows:

$$s_{i1} = g_{i1}^{-1}\left(x_{i1} - x_{i1d}\right) \tag{64}$$

In the equation, $x_{i1d} = [\overline{\theta}_{mi}, \overline{\varphi}_{vmi}]^T$ is the instruction of the trajectory inclination angle and trajectory deflection angle after filtering. Taking the derivative of s_{i1},

$$\dot{s}_{i1} = x_{i2} + g_{i1}^{-1}\left(d_{i1} - \dot{x}_{i1d}\right) \tag{65}$$

According to the dynamic surface sliding-mode control method and FTDO estimated value $\widehat{d}_{i1}$, the virtual control of the first dynamic surface is selected as

$$x_{i2}^{*} = g_{i1}^{-1}\left(-\widehat{d}_{i1} + \dot{x}_{i1d}\right) - k_{i1}s_{i1} \tag{66}$$

In the equation, $\dot{x}_{i1d}$ is the differential of the trajectory inclination angle and trajectory deflection angle after filtering, and $k_{i1} = \mathrm{diag}\{k_{i11}, k_{i12}\}$ is the positive definite matrix. The value of x_{i2}^{*} is obtained through the first-order low-pass filter, and the virtual control after filtering and its differential are given by

$$\begin{aligned} \tau_{i2}\dot{\overline{x}}_{i2}^{*} + \overline{x}_{i2}^{*} &= x_{i2}^{*}, \\ \overline{x}_{i2}^{*}(0) &= x_{i2}^{*}(0) \\ \dot{\overline{x}}_{i2}^{*} &= -\tau_{i2}^{-1}\left(\overline{x}_{i2}^{*} - x_{i2}^{*}\right) \end{aligned} \tag{67}$$

In the equation, $\tau_{i2} = \mathrm{diag}\{\tau_{i21}, \tau_{i22}\}$ is the time constant of the filter.

(2) The second dynamic error surface is defined by

$$s_{i2} = x_{i2} - \overline{x}_{i2}^{*} \tag{68}$$

In the equation, $\overline{x}_{i2}^{*}$ is the command signal after filtering. Taking the derivative of s_{i2},

$$\dot{s}_{i2} = f_{i2}\left(x_{i2}\right) + g_{i2}\left(x_{i2}\right)x_{i3} + d_{i2} - \dot{\overline{x}}_{i2}^{*} \tag{69}$$

According to the dynamic surface sliding-mode control method and FTDO estimated value $\widehat{d}_{i2}$, the virtual control of the first dynamic surface is given by

$$x_{i3}^{*} = g_{i2}^{-1}\left(x_{i2}\right)\left[-f_{i2}\left(x_{i2}\right) - \widehat{d}_{i2} + \dot{\overline{x}}_{i2}^{*} - k_{i2}s_{i2}\right] \tag{70}$$

In the equation, $\dot{\overline{x}}_{i2}^{*}$ is the instruction differential after filtering, and $k_{i2} = \mathrm{diag}\{k_{i21}, k_{i22}\}$ is the positive definite matrix. The value of x_{i3}^{*} is obtained through the first-order low-pass filter, and the virtual control after filtering and its differential can be obtained as follows:

$$\begin{aligned} \tau_{i3}\dot{\overline{x}}_{i3}^{*} + \overline{x}_{i3}^{*} &= x_{i3}^{*}, \\ \overline{x}_{i3}^{*}(0) &= x_{i3}^{*}(0) \\ \dot{\overline{x}}_{i3}^{*} &= -\tau_{i3}^{-1}\left(\overline{x}_{i3}^{*} - x_{i3}^{*}\right) \end{aligned} \tag{71}$$

In the equation, $\tau_{i3} = \mathrm{diag}\{\tau_{i31}, \tau_{i32}\}$ is the time constant of the filter.

(3) The third dynamic error surface is defined as follows:

$$s_{i3} = x_{i3} - \overline{x}_{i3}^{*} \tag{72}$$

In the equation, $\overline{x}_{i3}^{*}$ is the command signal after filtering. Taking the derivative of s_{i3},

$$\dot{s}_{i3} = f_{i3}\left(x_{i2}, x_{i3}\right) + g_{i3}u_i + d_{i3} - \dot{\overline{x}}_{i3}^{*} \tag{73}$$

According to the sliding-mode reaching law (see (59)), and FTDO estimated value $\widehat{d}_{i3}$, the "follower" dynamic surface sliding-mode control law is designed as follows:

$$\begin{aligned} u_i = g_{i3}^{-1}\Big[&-f_{i3}\left(x_{i2}, x_{i3}\right) - \widehat{d}_{i3} + \dot{\overline{x}}_{i3}^{*} - k_{i3}s_{i3} \\ &- k_{i4}\left|s_{i3}\right|^{\partial_{i3}}\mathrm{sgn}\left(s_{i3}\right)\Big] \end{aligned} \tag{74}$$

In the equation $\dot{\overline{x}}_{i3}^{*}$ is the instruction differential after filtering, $k_{i3} = \mathrm{diag}\{k_{i31}, k_{i32}\}$ and $k_{i4} = \mathrm{diag}\{k_{i41}, k_{i42}\}$ are the positive definite matrices, $\partial_{i3} = \mathrm{diag}\{\partial_{i31}, \partial_{i32}\}$, and $0 < \partial_{i3} < 1$.

It can be learnt by referring to (27)–(44) that the stability of the control algorithm of the interceptor "follower" can be guaranteed by selecting appropriate parameters.

6. Simulation Verification

To verify the effectiveness of the distributed cooperative IGC algorithm of the multi-interceptor with state coupling designed in this study, it is assumed that the flight velocity of the interceptor "leader" remains the same. According to the global communication topology structure shown in Figure 1 and the local communication topology structure shown in Figure 2, Figure 1 assumes that the "leader" can communicate with the remaining three "followers," while the "followers" can communicate with each other. Figure 2 assumes that the "leader" can only communicate with "follower 1," while "followers" can communicate with each other. The initial conditions of interceptor "leader," "follower," and target are listed in Table 1.

Focusing on the two communication topology structures shown in Figures 1 and 2, a simulation study is conducted for the cooperative IGC algorithm of the multi-interceptor with state coupling designed in this study. It is assumed

Table 1: Initial conditions of the leader, follower, and target.

No.		Parameter	Value	Parameter	Value	Parameter	Value	Parameter	Value
1	Leader	x_{m0}	0m	y_{m0}	0m	z_{m0}	0m	V_{m0}	800 m/s
2	Follower1	x_{m10}	600m	y_{m10}	0m	z_{m10}	500m	V_{m10}	800 m/s
3	Follower2	x_{m20}	800m	y_{m20}	0m	z_{m20}	1000m	V_{m20}	800 m/s
4	Follower3	x_{m30}	400m	y_{m30}	0m	z_{m30}	-500m	V_{m30}	800 m/s
5	Target	x_{t0}	4000m	y_{t0}	5000m	z_{m40}	3000m	V_{t0}	400 m/s

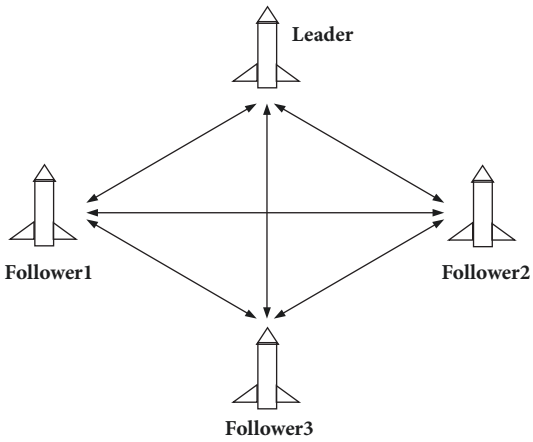

Figure 1: Global communication topology structure of interceptor "leader" and "follower".

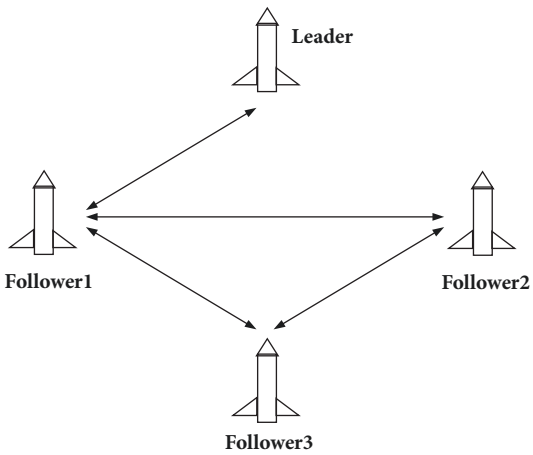

Figure 2: Local communication topology structure of the interceptor "leader" and "follower".

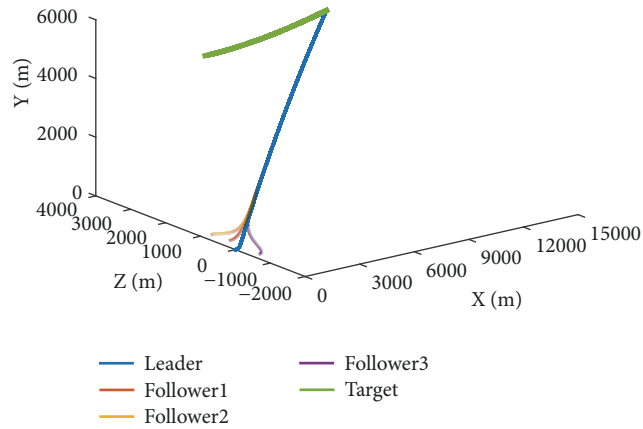

Figure 3: Motion trails of the interceptor "leader," "follower," and target in the global communication topology: X denotes the horizontal motion trail of the interceptor and target, Y denotes the longitudinal motion distance of the interceptor and target, and Z denotes the lateral motion trail of the interceptor and target.

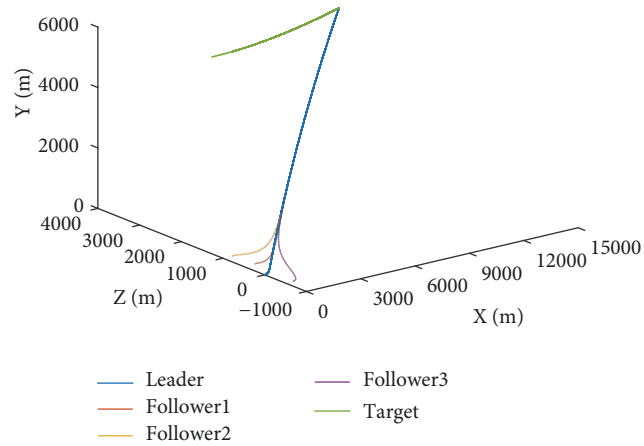

Figure 4: Motion trails of the interceptor "leader," "follower," and target in the local communication topology. X denotes the horizontal motion trail of the interceptor and target, Y denotes the longitudinal motion distance of the interceptor and target, and Z denotes the lateral motion trail of the interceptor and target.

that the disturbance of the system is $d_2 = d_3 = d_{i1} = d_{i2} = d_{i3} = 0.02\sin(t)$, and the intercepted target has a linear acceleration of $a_{t\varepsilon} = a_{t\beta} = 5m/s^2$. The comparison of the simulation results of the cooperative IGC algorithm of the multi-interceptor with state coupling in the global and local communication topology is given, as shown in Figures 3–11.

Figures 3 and 4 show the motion trail of the interceptor "leader," "follower," and target in the local and global communication topologies. It can be seen that the motion trail of the interceptor "follower" in two different communication topologies is gradually consistent with that of the "leader." Eventually, the "leader" and "follower" hit the target at the same time. The motion trail curve is smooth, showing short interception duration, fast convergence speed, and good stability.

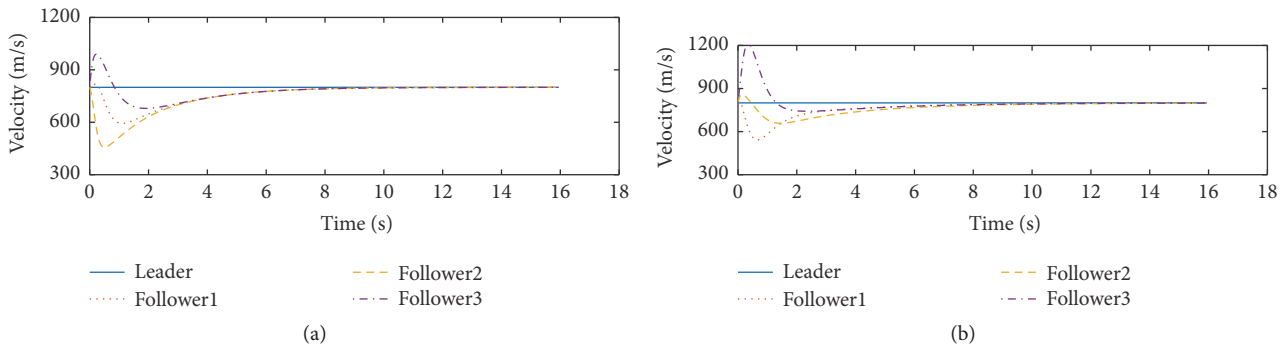

Figure 5: Interceptor velocity curve in the global and local communication topologies: (a) velocity curve in the global communication topology; (b) velocity curve in the local communication topology.

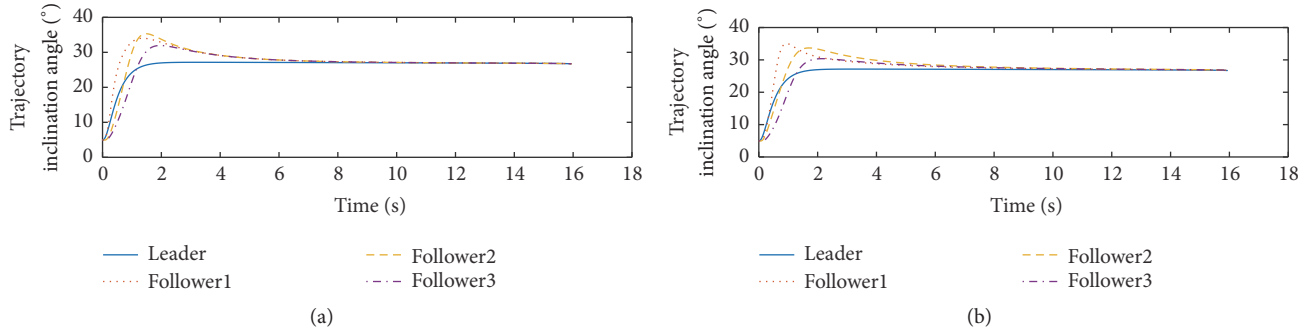

Figure 6: Trajectory inclination angle curve in the global and local communication topologies: (a) trajectory inclination angle curve in the global communication topology; (b) trajectory inclination angle curve in the local communication topology.

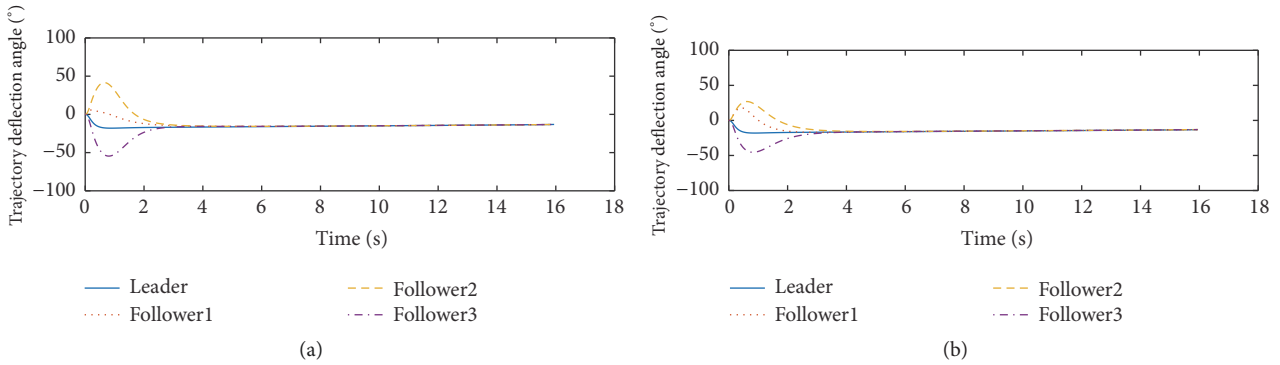

Figure 7: Trajectory deflection angle curve in the global and local communication topology: (a) trajectory deflection angle curve in global communication topology; (b) trajectory deflection angle curve in local communication topology.

Figures 5(a) and 5(b) show the velocity curve of the interceptor in the global and local topologies, from which it can be seen that the interceptor "follower" features a considerable overstriking property in the initial stage due to the lack of "leader." The convergence rate is slower than that in the global topology, but it can eventually reach the steady state of the "leader." The convergence process changes smoothly, and it shows good robustness to external disturbance. Similarly, it is clear from Figures 6–11 that the interceptor "follower" in the global and local communication topologies realizes the tracking of control instruction of the "leader." The convergence process is relatively smooth, and it also shows good robustness to external disturbance.

It can be seen from the simulation results of the global and local communication topologies that the distributed cooperative IGC algorithm of the multi-interceptor with state coupling designed in this study completes the tracking the instructions of the cooperative control strategy in the two different topologies and eventually achieves cooperative target interception.

The cooperative IGC algorithm of the multi-interceptor with state coupling proposed in this study and the traditional

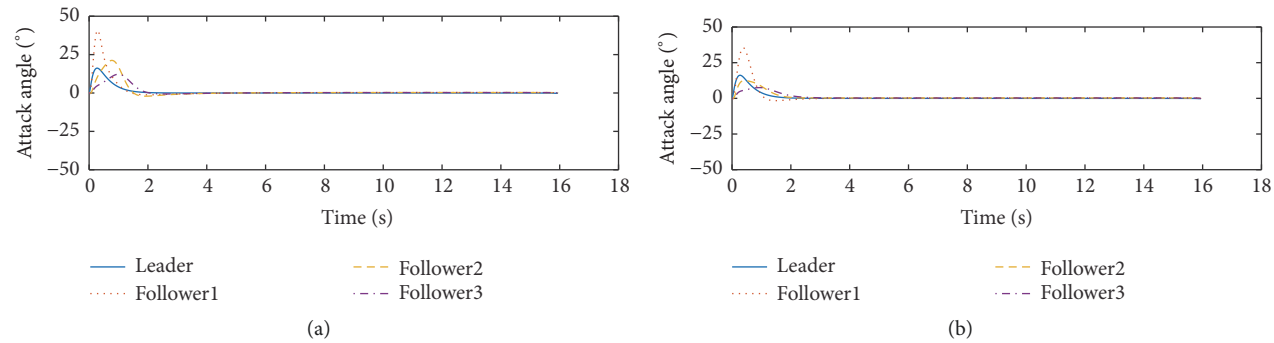

Figure 8: Attack angle curve in the global and local communication topologies: (a) attack angle curve in the global communication topology; (b) attack angle curve in the local communication topology.

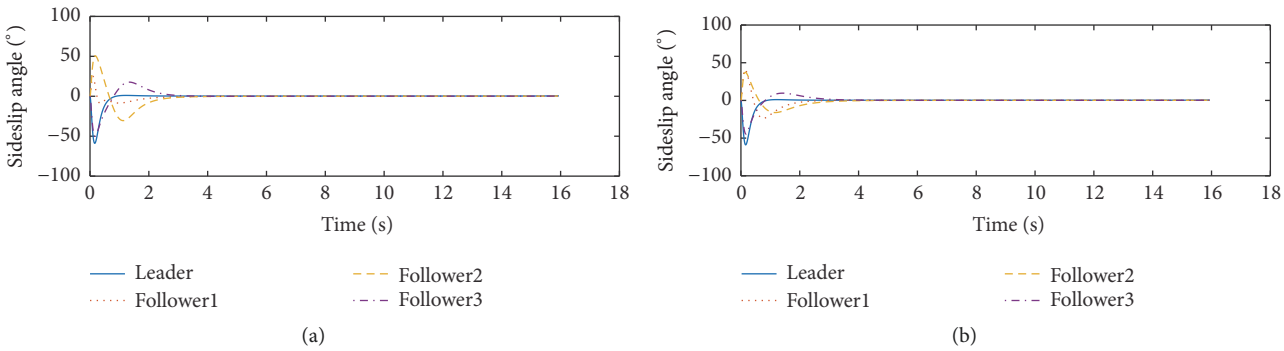

Figure 9: Sideslip angle curve in the global and local communication topologies: (a) sideslip angle curve in the global communication topology; (b) sideslip angle curve in the local communication topology.

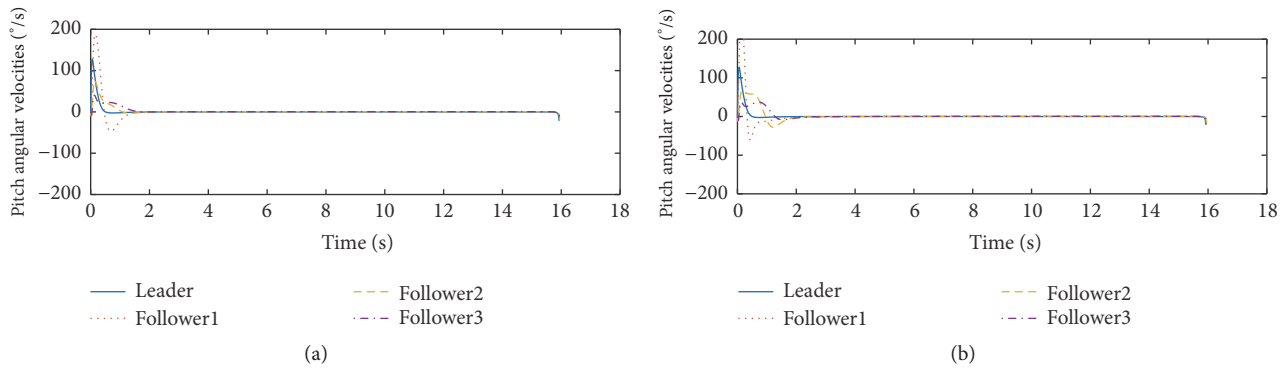

Figure 10: Pitch angular velocities curve in the global and local communication topologies: (a) pitch angular velocities curve in the global communication topology; (b) pitch angular velocities curve in the local communication topology.

method for multi-interceptor cooperation without state coupling are compared through numerical simulations. Figures 12 and 13 show the comparison results.

Figures 12 and 13 present the comparison of the attack and sideslip angle curves associated with the cooperative IGC algorithm of the multi-interceptor with state coupling and the traditional method for the multi-interceptor cooperation without state coupling. The convergence process associated with the cooperative IGC algorithm of the multi-interceptor with state coupling appeared to be smoother compared to that associated with the traditional method for the multi-interceptor cooperation without state coupling. The section of the curve after t = 4s particularly revealed more stable angle and sideslip angle curves using the state-coupled design methods. In contrast, fluctuations in the attack and sideslip angle curves were observed for the traditional design methods without state coupling. In other words, the cooperative IGC algorithm of the multi-interceptor with state coupling exhibited better resistance to interference and allowed for a more stable control of the interceptor

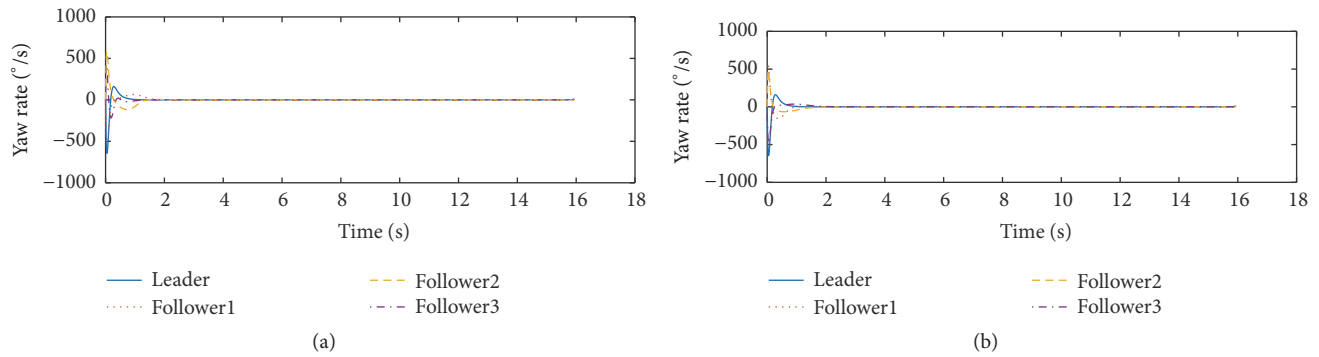

Figure 11: Yaw rate curve in the global and local communication topologies: (a) yaw rate curve in the global communication topology; (b) yaw rate curve in the local communication topology.

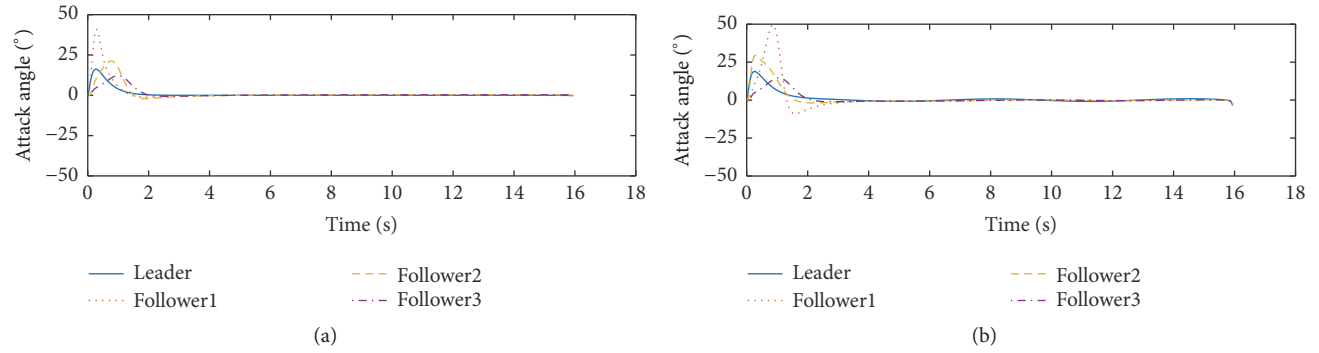

Figure 12: Comparison of the interceptor's attack angle curves in the design methods with and without state coupling: (a) attack angle curve in the design method with state coupling; (b) attack angle curve in the design method without state coupling.

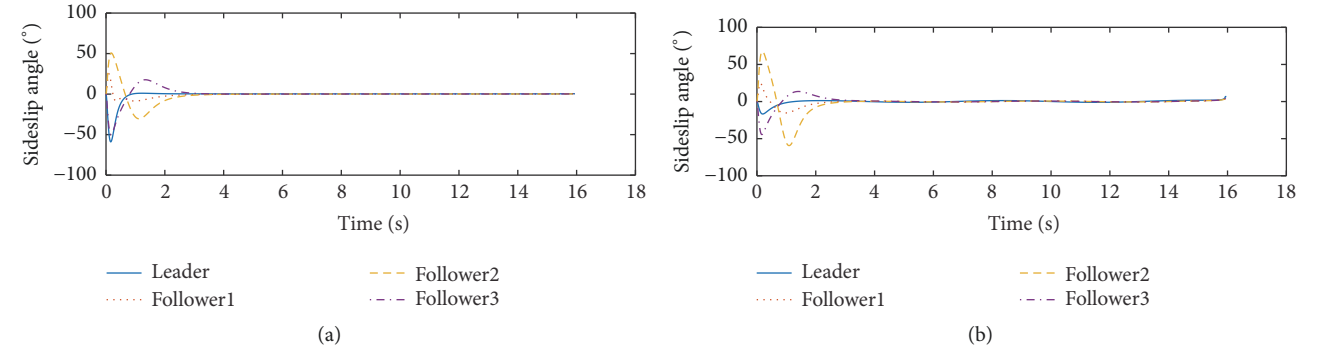

Figure 13: Comparison of the interceptor's sideslip angle curves in the design methods with and without state coupling: (a) sideslip angle curve in the design method with state coupling; (b) sideslip angle curve in the design method without state coupling.

compared to the traditional method without state coupling.

7. Conclusions

This study focused on the cooperative target interception by multi-interceptor and designed cooperative IGC algorithm of the multi-interceptor with state coupling "leader-follower" structure. The algorithm is designed by considering the coupling relation between the pitch and yaw channels of the interceptor. Further, this study combines the IGC method and introduces the distributed cooperative control strategy. The interceptor "leader" and "follower" control algorithm is designed separately by employing the dynamic surface sliding-mode control law and FTDO. The distributed cooperative control strategy guarantees that the "leader" and "follower" can hit the targets at the same time. The algorithm displays ideal trajectory characteristics in the simulation verification, and it can realize the cooperative interception of targets in both the global and local communication

topologies. Furthermore, the study provides a design method for the cooperative target interception of the multi-interceptor, with certain engineering values.

Notations

V_m, V_{mi}: Interceptor velocity
V_t: Target velocity
α, α_i: Attack angle
β, β_i: Sideslip angle
ω_y, ω_{yi}: Yaw rate
ω_z, ω_{zi}: Pitch angular velocity
$\varphi_{vm}, \varphi_{vmi}$: Trajectory deflection angle of interceptor
ρ: Air density
θ_m, θ_{mi}: Trajectory inclination angle of interceptor
θ_t: Trajectory inclination angle of target
$C_y^{\alpha}, C_y^{\alpha_i}$: Contribution to lift due to angle of attack α
$C_z^{\beta}, C_z^{\beta_i}$: Contribution to yaw force due to sideslip angle β
g: Acceleration due to gravity
J_y: Moment of inertia around the yaw axis
J_z: Moment of inertia around the pitch axis
$\overline{L}$: Reference length
m: Interceptor mass
$m_z^{\alpha}, m_z^{\alpha_i}$: Contribution to pitch moment due to angle of attack α
$m_y^{\beta}, m_y^{\beta_i}$: Contribution to yaw moment due to sideslip angle β
$m_y^{\omega_y}, m_y^{\omega_{yi}}$: Contribution to yaw moment due to yaw rate ω_y
$m_z^{\omega_z}, m_z^{\omega_{zi}}$: Contribution to pitch moment due to pitch rate ω_y
M_y, M_{yi}: Yaw moment
M_z, M_{zi}: Pitch moment
q: Dynamic pressure
q_β: Elevation angle
q_ε: Horizontal sight angle
r: Relative distance
S: Reference area
v_r: Relative velocity
v_β: Tangential relative velocity normal to yaw line-of-sight(YLOS)
v_ε: Tangential relative velocity normal to pitch line-of-sight(PLOS)
P_i: Motor power
$a_{m4\varepsilon}, a_{m4\beta}$: Longitudinal and lateral motion acceleration
$a_{t\varepsilon}, a_{t\beta}$: Longitudinal and lateral motion acceleration of the target
$a_{m3\varepsilon}, a_{m3\beta}$: Longitudinal and lateral acceleration.

Data Availability

The data used to support the findings of this study are available from the corresponding author upon request.

Conflicts of Interest

The authors declare that there are no conflicts of interest regarding the publication of this paper.

Acknowledgments

The authors gratefully acknowledge the suggestions and help by the Professor Xiaogeng Liang and Northwestern Polytechnical University. This work was supported by the Aeronautical Science Foundation of China [Grant no. 2016ZC12005].

References

[1] J. B. Zhao and S. X. Yang, "Review of muti-missile cooperative guidance," *Acta Aeronautica et Astronautica Sinica*, vol. 38, no. 1, pp. 1–13, 2017.

[2] I.-S. Jeon, J.-I. Lee, and M.-J. Tahk, "Homing guidance law for cooperative attack of multiple missiles," *Journal of Guidance, Control, and Dynamics*, vol. 33, no. 1, pp. 275–280, 2010.

[3] J.-I. Lee, I.-S. Jeon, and M.-J. Tahk, "Guidance law to control impact time and angle," *IEEE Transactions on Aerospace and Electronic Systems*, vol. 43, no. 1, pp. 301–310, 2007.

[4] N. Harl and S. N. Balakrishnan, "Impact time and angle guidance with sliding mode control," *IEEE Transactions on Control Systems Technology*, vol. 20, no. 6, pp. 1436–1449, 2012.

[5] D. Cho, H. J. Kim, and M.-J. Tahk, "Nonsingular sliding mode guidance for impact time control," *Journal of Guidance, Control, and Dynamics*, vol. 39, no. 1, pp. 61–68, 2016.

[6] M. Nikusokhan and H. Nobahari, "Closed-form optimal cooperative guidance law against random step maneuver," *IEEE Transactions on Aerospace and Electronic Systems*, vol. 52, no. 1, pp. 319–336, 2016.

[7] V. Shaferman and T. Shima, "Cooperative differential games guidance laws for imposing a relative intercept angle," *Journal of Guidance, Control, and Dynamics*, vol. 40, no. 10, pp. 2465–2480, 2017.

[8] X. Wang, Y. Zheng, and H. Lin, "Integrated guidance and control law for cooperative attack of multiple missiles," *Aerospace Science and Technology*, vol. 42, pp. 1–11, 2015.

[9] S. R. Kumar and D. Ghose, "Cooperative Rendezvous Guidance using Sliding Mode Control for Interception of Stationary Targets," *IFAC Proceedings Volumes*, vol. 47, no. 1, pp. 477–483, 2014.

[10] J. Zhao and S. Yang, "Integrated cooperative guidance framework and cooperative guidance law for multi-missile," *Chinese Journal of Aeronautics*, vol. 31, no. 3, pp. 546–555, 2018.

[11] T. Lyu, Y. Lyu, and C. Li, "Cooperative guidance with impact angle constraint based on leader-follower strategy," *Advances in the Astronautical Science*, vol. 160, pp. 4009–4025, 2017.

[12] Q. Zhao, J. Chen, X. Dong, Q. Li, and Z. Ren, "Cooperative guidance law for heterogeneous missiles intercepting hypersonic weapon," *Hangkong Xuebao/Acta Aeronautica et Astronautica Sinica*, vol. 37, no. 3, pp. 936–948, 2016.

[13] V. Shaferman and T. Shima, "Cooperative optimal guidance laws for imposing a relative intercept angle," *Journal of Guidance, Control, and Dynamics*, vol. 38, no. 8, pp. 1395–1408, 2015.

[14] P. K. Menon and E. J. Ohlmeyer, "Integrated design of agile missile guidance and autopilot systems," *Control Engineering Practice*, vol. 9, no. 10, pp. 1095–1106, 2001.

[15] Y. B. Shtessel and C. H. Tournes, "Integrated higher-order sliding mode guidance and autopilot for dual-control missiles," *Journal of Guidance, Control, and Dynamics*, vol. 32, no. 1, pp. 79–94, 2009.

[16] M. Cross and Y. B. Shtessel, "Integrated Guidance Navigation and Control Using High-Order Sliding Mode Control for a Missile Interceptor," in *Proceedings of the 2018 AIAA Guidance, Navigation, and Control Conference*, Kissimmee, Florida.

[17] S. Shamaghdari, S. K. Nikravesh, and M. Haeri, "Integrated guidance and control of elastic flight vehicle based on robust MPC," *International Journal of Robust and Nonlinear Control*, vol. 25, no. 15, pp. 2608–2630, 2015.

[18] Z. Zhu, D. Xu, J. Liu, and Y. Xia, "Missile guidance law based on extended state observer," *IEEE Transactions on Industrial Electronics*, vol. 60, no. 12, pp. 5882–5891, 2013.

[19] T. Yamasaki, S. N. Balakrishnan, and H. Takano, "Integrated guidance and autopilot design for a chasing UAV via high-order sliding modes," *Journal of The Franklin Institute*, vol. 349, no. 2, pp. 531–558, 2012.

[20] H. Zhou, H. Zhao, H. Huang, and X. Zhao, "Integrated guidance and control design of the suicide UCAV for terminal attack," *Journal of Systems Engineering and Electronics*, vol. 28, no. 3, pp. 546–555, 2017.

[21] B. Panchal, K. Subramanian, and S. E. Talole, "Robust Integrated Guidance and Control Design for Tactical Missiles," in *Proceedings of the 2018 AIAA Guidance, Navigation, and Control Conference*, Kissimmee, Florida.

[22] S. H. Seyedipour, M. F. Jegarkandi, and S. Shamaghdari, "Nonlinear integrated guidance and control based on adaptive backstepping scheme," *Aircraft Engineering and Aerospace Technology*, vol. 89, no. 3, pp. 415–424, 2017.

[23] F.-K. Yeh, "Design of nonlinear terminal guidance/autopilot controller for missiles with pulse type input devices," *Asian Journal of Control*, vol. 12, no. 3, pp. 399–412, 2010.

[24] J. Wang, L. Liu, T. Zhao, and G. Tang, "Integrated guidance and control for hypersonic vehicles in dive phase with multiple constraints," *Aerospace Science and Technology*, vol. 53, pp. 103–115, 2016.

[25] Huibo Zhou, Shenmin Song, Junhong Song, and Jing Niu, "Design of Second-Order Sliding Mode Guidance Law Based on the Nonhomogeneous Disturbance Observer," *Journal of Control Science and Engineering*, vol. 2014, pp. 1–10, 2014.

[26] Bhavnesh Panchal and S. E. Talole, "Generalized ESO and Predictive Control Based Robust Autopilot Design," *Journal of Control Science and Engineering*, vol. 2016, pp. 1–12, 2016.

[27] Y. B. Shtessel, I. A. Shkolnikov, and A. Levant, "Smooth second-order sliding modes: missile guidance application," *Automatica*, vol. 43, no. 8, pp. 1470–1476, 2007.